Journal of Materials Chemistry A

Challenge-Driven Printing Strategies Toward High-Performance Solid-State Lithium Batteries

Journal:	*Journal of Materials Chemistry A*
Manuscript ID	TA-REV-10-2021-009322.R1
Article Type:	Review Article
Date Submitted by the Author:	24-Dec-2021
Complete List of Authors:	Wang, Jing; The University of Chicago Huang, Xingkang; The University of Chicago Chen, Junhong; The University of Chicago, Pritzker School of Molecular Engineering

ARTICLE

Challenge-Driven Printing Strategies Toward High-Performance Solid-State Lithium Batteries

1`Received 00th January 20xx,
Accepted 00th January 20xx

DOI: 10.1039/x0xx00000x

Jing Wang,[a,b] Xingkang Huang, [a,b] and Junhong Chen *,[a,b]

Solid-state lithium batteries (SSLBs) are promising candidates for replacing traditional liquid-based Li-ion batteries and revolutionizing battery systems for electric vehicles and portable devices. However, longstanding issues such as form factors, interfacial contact resistance, balance between ion conductivity and mechanical strength, and manufacturing processability limit their applications. In this review we present how advanced printing technologies can help to mitigate typical problems in main components of SSLBs and improve device performance. We first introduce the common printing techniques for energy storage devices, then focus on the issues and corresponding printing strategies for anodes, cathodes, and solid-state electrolytes to guide the construction of energy-dense, free-form SSLBs. The features and effects of the printed structures are emphasized, as well. We conclude by discussing the problems associated with printing technologies and the potential research directions for printed solid-state batteries.

1. Introduction

Due to the rapid development and extensive use of electric vehicles and smart grids, there is a growing demand for reliable and cost-effective energy storage devices.[1-3] Among the various portable power sources, lithium (Li)-ion batteries have received the most attention at both the scientific and applied levels due to their high specific capacity and design versatility.[4-6] In the past few decades, organic liquid electrolytes have been widely used for lithium batteries, which offer the benefits of high ionic conductivity and excellent wettability toward electrode surfaces. However, their relatively low energy density and thermal stabilities have led to several safety issues and thus limit their applications in next-generation flexible and wearable electronic devices.[7-9] Li has a low reaction potential (3.045 V vs. standard hydrogen electrode) and a high theoretical capacity (3,860 mA h g^{-1}), providing a much higher energy density for next-generation batteries than existing graphite anodes.[10] The use of Li as an anode also enables Li-free, high-capacity cathode candidates such as sulfur and oxygen;[11-13] however, the growth of Li dendrites on Li electrodes may punctuate the conventional polymer separators, creating a shortage which then generates heat and possibly ignites the flammable liquid electrolytes, resulting in runaway.[14] Thus, solid-state electrolytes (SSEs) emerged to address these issues by minimizing the possibility of punctuating Li dendrites and to improve safety by eliminating the organic electrolytes. With the benefits provided by SSEs, SSLBs can meet the requirements for higher specific energy density, longer cycle life, and better safety for the Internet of Things (IoT).[15]

SSEs can be catalogued as an inorganic solid electrolyte (ISE), solid polymer electrolyte (SPE), and composite polymer electrolyte (CPE).[16-18] To achieve high-performance SSLBs, SSE properties should possess high ion conductivity (>10^{-4} S cm^{-1}), negligible electronic conductivity (<10^{-12} S cm^{-1}), a wide electrochemical window, good chemical stability, and excellent mechanical strength. Unfortunately, there are formidable obstacles limiting the realization of ideal SSEs, such as inherently poor ion conductivity at room temperature, a complicated fabrication process, large resistance at the interface between the SSEs and active materials, and chemical stability issues with the electrodes.[19-21] SSEs play an important role in effectively suppressing the dendrite formation on lithium anodes, but new problems such as unfavorable side reactions at the interface and significant volume change have arisen.[21] Additionally, it is not impossible that dendrite growth can penetrate through the cross-linked network structure of soft SPEs, especially at a high current density. Besides the anodes, a high mass-loading or thick cathode is crucial for improving energy density and accelerating the commercialization of SSLBs. Nevertheless, achieving high loadings is quite difficult for cathodes (i.e., S and Li_2S) with poor electronic conductivity, which notoriously suffer from sluggish kinetics and point-to-point contacts with SSEs.

It has been shown that combining rational material design with advanced nanotechnology results in powerful strategies to solve these problems at the nanoscale and fundamental chemistry level.[14,22] However, the application of these strategies in practice for large-scale manufacturing and monolithic integration with other functional devices is limited by the tortuous material handling procedures, special chemical bath requirements, and difficulty in controlling thickness and uniformity. It should also be noted that the structures of the bulk electrodes and electrolytes have a profound effect on the overall performance of the batteries, but conventional

[a] Pritzker School of Molecular Engineering, University of Chicago, Chicago, Illinois 60637, USA.
[b] Chemical Sciences and Engineering Division, Physical Sciences and Engineering Directorate, Argonne National Laboratory, Lemont, Illinois 60439, USA.
† Footnotes relating to the title and/or authors should appear here.
Electronic Supplementary Information (ESI) available: [details of any supplementary information available should be included here]. See DOI: 10.1039/x0xx00000x

fabrication processes are too elaborate to achieve complex shapes or configuration designs with high-aspect-ratio 3D architectures. These problems were difficult to solve until the emergence of additive manufacturing, which has provided new methods and tools to facilely build versatile battery configurations at a large scale.[23-26] Besides the benefits of arbitrary structural designs and scalable manufacturing processes, additive manufacturing offers innovative solutions to the problems with SSLBs by carefully matching the printable materials and printing techniques.

Here we review the field of additive manufacturing for SSLBs by examining their promise to alleviate typical problems in engineering SSLBs, as well as the issues associated with printing themselves. It is believed that various printing techniques will help to promote the development of solid-state lithium batteries by solving their key problems: dendrite growth and large volume change in the Li anode, sluggish ion and electron transport in the cathode, complicated fabrication processes for ideal SSEs, and interfacial issues between the SSE and electrodes. In this review we first briefly introduce the development and recent progress of different types of printing techniques for SSLBs, followed by a discussion of the issues with SSLBs and the corresponding printing strategies toward improving their performance. Finally, the key challenges and opportunities for constructing high-performance solid-state lithium batteries via printing technologies are proposed.

2. Major printing techniques for solid-state batteries

As a convenient approach for pattern design and large-scale production, there is increasing interest in the application of printing technologies for energy storage devices. Various printing techniques have been invented, developed, used, and improved in recent years.[25,27,28] The selection of printing techniques depends on the desired materials, processability of the inks, resolutions, pattern dimensions, and the specific performance requirements for the final products. In this section, we briefly introduce representative advanced printing techniques that are frequently exploited for fabricating high-performance batteries, in combination with the corresponding material selection and ink properties for each printing technique.

Inkjet printing (IJP) is a droplet-based, non-contact, and mask-free deposition technique that has a high resolution and multi-material printing capability (Fig. 1a). A desired pattern can be directly formed by propelling microdroplets of the printable inks through a movable nozzle onto various substrates. A wide range of materials including polymers, metals, biomaterials, nanoparticles have been employed for IJP. The inks can be prepared by dispersing the active materials into a solvent with additives. To be printable and stable, the inks should meet the specific requirements for density ρ, surface tension σ, and dynamic viscosity μ; this typically ensures $1<Z<10$, where Z is the inverse Ohnesorge number. The inks are usually in a diluted liquid form with low viscosity and active material loading. Due to the properties of the inks, the printed patterns tend to be thin films with limited height-zone design versatility. The major issues with IJP include the frequent clogging of narrow nozzles due to the aggregation of active materials in the ink, as well as the relatively slow printing yield. Considering the high resolution and wide range of printable materials, inkjet printing is commonly used in the fabrication of thin-film types of electrodes for micro batteries.[29-31]

Aerosol jet printing (AJP) is also a droplet-based and noncontact direct writing approach that does not require a predesigned mask (Fig. 1b). Similar to inkjet printing, AJP normally fabricates 2D thin films with high resolution, but the drop formation and delivery are quite different. In the AJP process the droplets are generated by ultrasonic atomization and their size can be reduced by solvent evaporation. Droplets with a diameter between 1–5 μm are then transported by aerosol gas to the deposition nozzle. Due to the special ink aerosolization and delivery approach, there is a wider range of printable materials and acceptable ink viscosities (1–1000 mPas) for AJP compared with IJP. Attributing to the drop on-demand techniques and processability of high-viscosity inks, AJP enables the fabrication of SSEs and forms seamless electrode/electrolyte interfaces.[32] Denier *et al.* printed polyethylene oxide (PEO)-based CPE directly on $LiFePO_4$ cathodes using AJP.[33] The printed layer was smooth, conformal, and conductive enough, with adequate permeation ability into the cathode bulk to form a low ionic-resistance interface.

Direct ink writing (DIW) is an extrusion-based 3D printing method with the advantages of easy operation, wide material range, cost effectiveness, and mask-free process. The ink for DIW must be viscoelastic with shear-thinning behavior, whereby the viscosity decreases with increasing shear rates. The paste-like ink is then extruded as continuous filaments to build the 3D architectures on a platform by stacking consecutive layers using computer-aided design (CAD) software (Fig. 1c). Factors like nozzle size, applied pressure, and ink properties together influence the resolution, which can reach 1 μm by optimizing the parameters. DIW is the most widely used printing approach for fabricating battery modules due to its material diversity, simple printing process, and low risk of nozzle clogging.[34-36] Moreover, the high-viscosity ink for DIW enables high active material loading in the printed 3D structure, which can significantly increase the areal capacity and energy density. However, preparing printable inks with sufficiently high yield stress and viscosity, shear-thinning behavior, and well controlled viscoelasticity is sophisticated.

ARTICLE

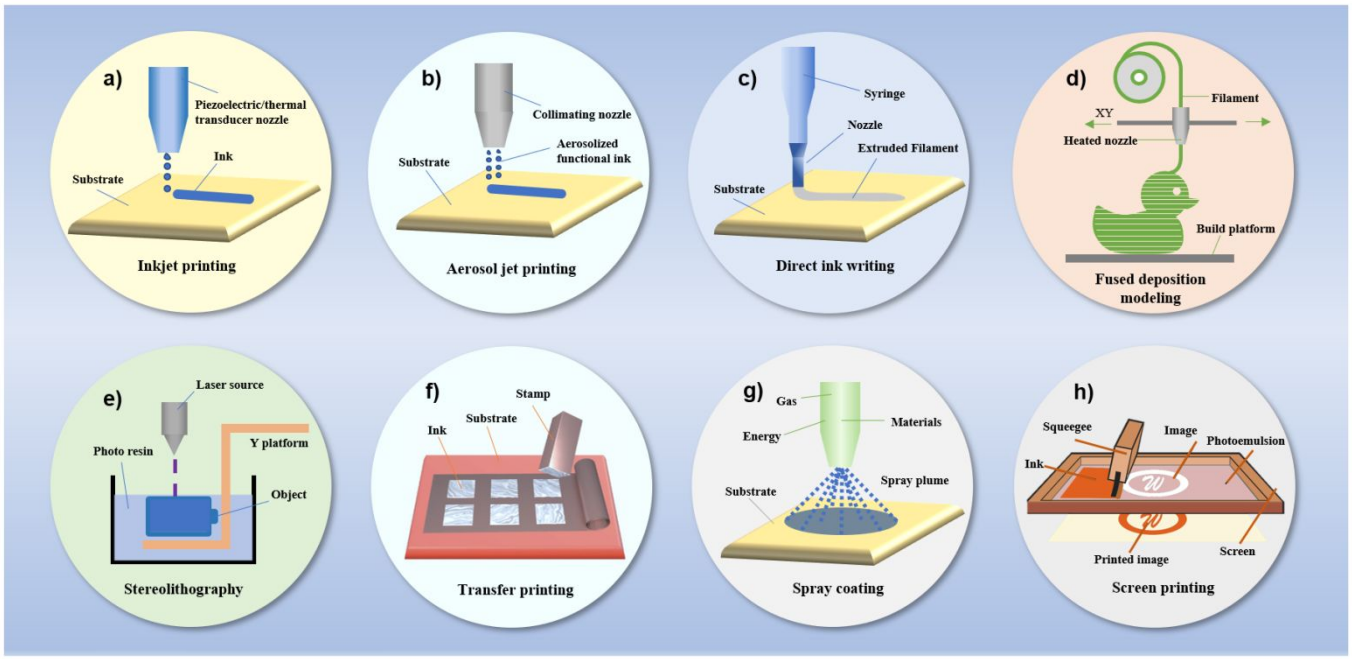

Figure 1. Overview of printing techniques for SSLBs: (a) Inkjet printing. (b) Aerosol jet printing. (c) Direct ink writing. (d) Fused deposition modelling. (e) Stereolithography. (f) Transfer printing.[44] Copyright (2021), Wiley-VCH GmbH. (g) Spray printing. (h) Screen printing.

Fused deposition modeling (FDM) is another common extrusion-based 3D printing technology (Fig. 1d). The 3D objects are created by depositing thermoplastic filaments at their glass transition state in a layer-by-layer style. The filaments will then be solidified quickly at room temperature or lower to form a uniform hardened 3D structure. To prepare the extrusion paste, thermoplastic materials should be used, including polycarbonate (PC), polyamide (PA), polylactic acid (PLA), and acrylonitrile butadiene styrene (ABS). Active materials are then incorporated into the thermoplastic matrix. To prepare the electrodes, conductive agents like graphene and carbon black can be added to improve the conductivity. The main advantages of FDM are low material waste, affordable prices, high production speed, and simple operation.[37-39] Golodnitsky *et al.* fabricated PEO-PLA based polymer electrolytes via a fused-deposition 3D printer.[40] A disc-shaped solid electrolyte with a diameter of 19 mm and a thickness of 200 µm was successfully printed with a relatively high ionic conductivity of 3×10^{-5} S/cm. However, its application in batteries is restricted by the low printing resolution (50–200 mm), lower flexibility of the multi-material capability, and low electrical conductivity due to the large portion of inactive electrochemical materials.

Stereolithography (SLA) is another promising 3D printing method based on solidifying photocurable resin using a beam of ultraviolet (UV) laser (Fig. 1e). The 3D structure is created layer by layer with a predesigned CAD pattern. During this process, proper photoinitiation process and fast cross-linking reaction are needed to form highly cross-linked networks upon exposure to the light. Therefore, to prepare the printable resins, active materials, compatible photoinitiators, and prepolymer materials are necessary. High resolution and very fine features (1 µm) can be achieved by rationally choosing the light source and suitable resins. The major challenges with SLA are complicated printable resin preparation, insufficient active materials diversity, residue from the photoinitiators, and uncured resin. However, compared with DIW and FDM, SLA is a real 3D structure creation technique that doesn't require building the structure in a layer-by-layer stacking fashion, and thus SLA has been widely used for fabricating complex 3D structures with a high-surface finish. According to the component of printable resin, SLA shows great potential for printing polymer-based SSEs with complex surface patterns or novel 3D hierarchical structures.[41-43]

Transfer printing (i.e., stamp printing) is a convenient 2D pattern fabrication method that transfers materials with a stamp from the donor (growth) substrate to the receiver substrate (Fig. 1f). Typically, the functional materials (e.g., nanomaterials) are prefabricated on the donor substrate. A stamp then picks up the ink on the donor substrate and brings it to the receiver. The successful transfer process hinges on the

interfacial adhesion at the interfaces of the ink/substrates and the stamp/ink. The adhesion strength at the stamp/ink interface should be larger than the ink/donor, which enables the ink to be transferred onto the stamp. Conversely, the adhesion strength at the stamp/ink interface should be smaller than the ink/receiver, allowing the ink to be peeled off onto the receiver. Due to its simple operation, cost-effectiveness, high reliability, and high efficiency, transfer printing can fabricate tiny, ultra-thin, and flexible batteries in high-throughput manner.[44] However, the adhesion requirement at the interfaces is hard to satisfy and the stamps should be designed according to the desirable printed patterns.

Spray printing is a quick and economical coating technique for defining 2D patterns by using a mask (Fig. 1g). The ink is divided into droplets via an atomization process and carried to arbitrary substrates in a mixture of gas and droplets. The atomization can be conducted by a high-velocity gas stream or a piezoelectric ultrasonic transducer. A heated substrate can accelerate the drying process, allowing another layer to be printed without interference. The resolution of the printed pattern depends on the ink components, nozzle dimensions, gas stream speed, drying process, and so on.[45-47] Due to the atomization and drying process, spray-printed patterns are normally porous.[48] Grant *et al.* prepared porous organic electrodes by the "layer-by-layer" spray-printing technique.[49] Active materials, carbon black, and two fugitive liquids were used to form the ink. The evaporation of solvents generated a honeycomb pore structure. A polymer SSE was then deposited directly onto the electrodes and well infiltrated through the porous electrodes. The as-fabricated organic symmetric solid-state batteries (SSBs) had a discharge cell voltage of more than 1 V with good cycling stability.

Screen printing is a conventional thin-film deposition technique (Fig. 1h). A liquid paste is typically made with active materials, conductive agents (e.g., graphite, carbon black), binders (e.g., resins or cellulose acetate), and solvents. The paste is then forced through a mesh screen mask by a squeegee to form a specific patten on the substrate. Though different masks are needed for different patterns, it is relatively easy to print the hollow patterns compared with other printing techniques. The simple ink preparation, user-friendly operation, and high production efficiency make screen printing a good tool to fabricate both electrodes and SSEs for batteries.[50-52]

3. Printing strategies for anodes

Due to its ultra-high specific capacity and low redox potential, lithium has been considered to be the most promising candidate for high-energy density batteries. Nevertheless, the inhomogeneous Li ion deposition during the plating/stripping process leads to uncontrollable lithium dendrite growth. The large volume changes give rise to the continuous consumption of electrolytes and breakage of the solid–electrolyte interphase (SEI). These side effects can eventually induce an internal short circuit and unsatisfactory electrochemical performance. SSEs with lithium that possess a rigid property and chemical stability may effectively mitigate these negative effects; however, the poor wettability of ISEs and the soft nature of SPEs could lead to the nonuniform distribution of Li^+ flux and increase safety risks.[53-55] The rational design of the lithium anode is still vitally important for SSBs to achieve reliable energy densities, maintain high Coulombic efficiency, and enhance cycling stability. Many strategies toward suppressing lithium dendrite and infinite volume change have been demonstrated, which generally include guiding Li nucleation by Li-M (where M refers to Sn, Si, and Mg, etc.) alloys, constructing novel 3D structures, and introducing protection layers. Despite these significant efforts, fabricating a form-factor free, thickness-controlled, and high-performance Li anode for practical applications remains challenging. Printing techniques provide an uncomplicated, economic, and scalable approach to constructing versatile architectures for Li anodes with controllable morphologies, thereby bridging the gap between theoretical speculation and practical trials.

Printing 3D Li anodes or 3D scaffolds for Li storage is an effective strategy for solving the previously described problems with Li anodes. The large specific surface of the 3D architectures can reduce local current density and thus facilitate uniform Li deposition. Besides, the stable, interconnected 3D structures accommodate massive Li and minimize volume change during the charging/discharging process, thus enhancing safety and cycling stability.[59-62] For instance, Ding *et al.* designed a robust 3D pure Cu framework (3DP-Cu) as the current collectors for an Li anode via DIW with a gel-link ink consisting of Cu particles and Pluronic F127 hydrogels.[63] A straightforward post-processing heat treatment was applied to decompose the Pluronic F127, generating microchannels. Benefiting from the porous network with a large number of electroactive sites, the 3DP-Cu enabled the dissipation of the local current density and inhibited the unwanted Li dendrite growth. More impressively, attributing to the mesh-like structure deliberately incorporated by 3D printing, the porous 3D Cu current collectors could withstand a high pressure of ~1.4 MPa, thus retaining the micron-sized pores without visible fractures during the sintering and assembly process. Compared with porous Cu coins prepared by a traditional ceramic process, the 3DP-Cu exhibited a significantly higher areal capacity (20 mA h cm^{-2}), a longer cycle life and better mechanical stability, thus presenting the advantages of printed structures as current collectors for uniform Li deposition.

ARTICLE

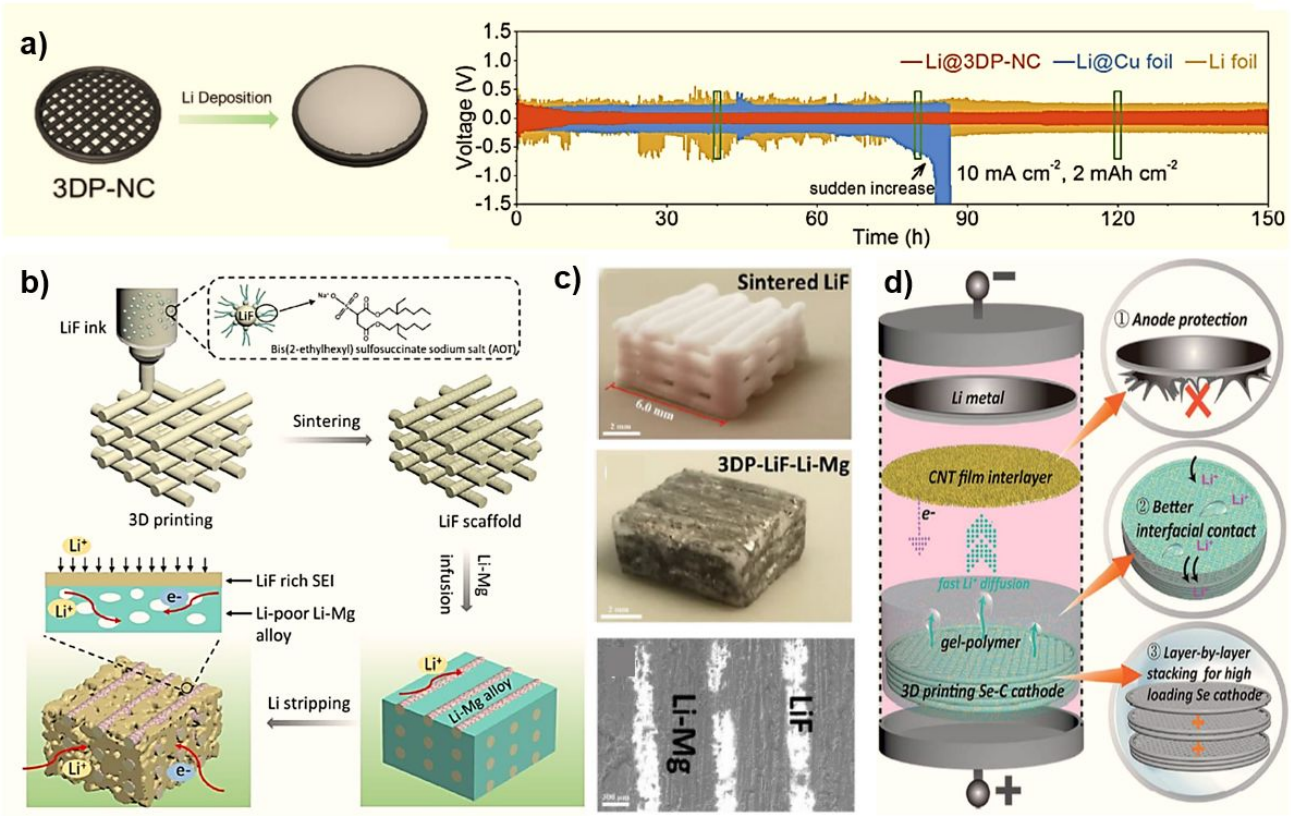

Figure 2. Selected examples of printed dendrite-free lithium metal anodes. (a) Schematic illustration of the Li plating process on 3DP-Cu (left) and galvanostatic cycling profiles of symmetric cells using the Li@3DP-NC, Li@Cu foil, and bare Li foil electrodes at the current rate of 10 mA cm^{-2} and a limited capacity of 2 mA h cm^{-2} (right). Reproduced with permission.[56] Copyright (2020), Elsevier Ltd. (b) Scheme of 3D printed LiF scaffolds. After drying and sintering, pure LiF scaffolds were infiltrated with molten Li-Mg alloy to form an Li anode, and (c) the digital photo of the 3D printed LiF scaffolds (upper), the digital photo of the 3DP-LiF-Li-Mg (middle), and SEM image of the 3DP-LiF-Li-Mg from top view (lower).[57] Copyright (2021), Elsevier Ltd. (d) Schematic illustration of 3D printed SSBs with CNTs as an interlayer for protecting Li metal.[58] Copyright (2020), Royal Society of Chemistry.

It is worth mentioning that printing 3D architectures with rational materials selection will bring additional effects toward the battery system.[64] Wang *et al.* employed 3D printing technology to design a porous N-doped carbon framework with a hierarchical porosity structure (Fig. 2a). The novel structure was designed by printing the Zn-metal organic framework (MOF) ink (ZIF-L crystals) and constructing a mesh-like architecture with stacked filaments, which created numerous large pores. With the decomposition of organic components and the volatilization of Zn metal during the post-treatment process, micro- and meso-pores were formed within the filaments. Impressively, the printed structure showed multiple advantages for enhancing the performance of the Li anode. The large-sized microchannels accommodated massive Li and suppressed the large volume change. The large surface area dissipated the high current density. The lithophilic N-doped carbon surface enabled a uniform nucleation for the Li to inhibit the unwanted dendrite growth.[56] As a result, the 3D printed N-doped carbon framework exhibited an ultrahigh areal capacity of 30 mA h cm^{-2} at a current density of 10 mA cm^{-2} together with highly stable Li plating/stripping behavior. By utilizing the benefits of DIW on facile fabrication of a complicated shape, Yang *et al.* printed a chemically stable LiF scaffold with order porosity for Li alloy anodes (Fig. 2b). The 3D-printed LiF scaffold maintained the structural integrity of the electrodes, even at a high temperature of 400 °C, and thus reliably minimized the volume change during the Li plating/ stripping process. Furthermore, the LiF scaffolds formed uniform LiF-rich SEI

layers, thus significantly enhancing Li^+ mobility at the Li anode/electrolyte interface. The Li-Mg alloy infiltrated in the porous 3D framework constituted the continuous conductive network and further promoted the uniform nucleation and growth of Li during cycling (Fig. 2c). The resulting dendrite-free anode exhibited a high areal capacity of 30 mA h cm^{-2} and a good deep Li stripping and plating property. Therefore, the tactical material selection and design combined with printing strategies would give rise to the synergistic effect of unique material properties and novel printed structures.[57]

Like the Li-Mg alloy, as previously discussed, a series of Li-M alloys have shown good potential in aiding the uniform Li nucleation process and boosting the performance of lithium metal batteries. Recently, Hu *et al.* fabricated an ultra-thin and flexible Li-Sn alloy anode with good electrochemical performance by stamp printing, in which various patterns were printed using the postmarks made from Cu stampers. The stamping approach can facilely make an Li alloy anode as thin as 15 μm, which avoids the overdose of Li and thus better matches the capacity of commercial cathode materials. The flexible Li-Sn anode from the stamp printing was assembled with a commercial NCM532 cathode in a pouch cell, which showed reliable performance and a high energy density of 615 Wh kg^{-1} after being folded repeatedly. Besides, this method can be readily extended to other alloy anodes as well as to versatile substrates with any shapes, which promotes the practical usage of dendrite-free Li anode in thin-film batteries.[44]

Printing an Li protective layer with good mechanical strength and stable chemical properties is also a promising method for suppressing Li dendrite growth and large volume expansion. Various printing techniques can ensure controllable thickness, a low-cost process, scalable methodology, and reliable performance.[65,66] For example, Sun *et al.* fabricated a dense and freestanding carbon nanotube (CNT) protective layer (200 μm in thickness and 10 mm in diameter) to protect the Li metal anode via a 3D printing and freeze-drying process (Fig. 2d). Compared with the symmetric coin cell without the CNT layer, the coin cell with the CNT layer presented a stable lifetime almost 10 times longer (800 h) and had a much lower overpotential (71 mV) during the stripping and plating process. In addition, a smooth surface was obtained without mossy-like Li deposition and Li corrosion during cycling was largely reduced, which was attributed to the uniform charge distribution and good structural protection provided by the dense CNT layer.[58]

Another property that should be equipped with protective layers is high Li-ion conductivity, as it is crucial for decreasing the overpotential induced by ion concentration differences. Pail *et al.* fabricated Li_3N@Cu nanowires by roll-pressing a Cu_3N thin layer (3 μm) onto a bare Li metal. The spontaneous conversion reaction between the Li and Cu_3N resulted in porous Li_3N@Cu nanowires on the electrode. In a symmetric cell test, a high areal capacity of 5.0 mA h cm^{-2} for 100 h at 5.0 mA cm^{-2} was achieved by the Li_3N@Cu–Li electrode, which is attributed to the stabilized Li metal surfaces due to the high Li ion conductivity ($\approx 10^{-3}$ S cm^{-1}) and low electronic conductivity ($<10^{-12}$ S cm^{-1}) of Li_3N. As a result, Li dendrite growth and dead Li formation were effectively suppressed.[67]

4. Printing strategies for cathodes

Increasing the thickness or the active material loading of a cathode is an attractive option for enhancing volumetric capacity and accelerating the realization of commercial applications of SSBs. A thick cathode with a high areal capacity will also help to balance the anode capacity and avoid large Li metal excess in the cell, which maximizes the utility of the materials and improves device performance. However, increasing the active material loadings of cathodes is especially challenging in SSBs, considering the sluggish ion transport kinetics at the interface between cathode and SSEs. The point-to-point contacts between the cathodes and the SSEs considerably limit the use of active material and require a large SSE fraction (30–50 wt.%) in the cathode composites to provide sufficient ionic diffusion, which results in the low volume fraction of the cathode.[68-70] Another serious issue with achieving high active material loading lies in the intrinsic poor conductivity and sluggish mass transport in most of the cathode materials (e.g., S and Li_2S) for SSBs. Therefore, establishing high-loading cathodes with satisfactory ion and electron transport kinetics is essential for improving the electrochemical performance of SSBs.

An ultra-thin cathode should have a rapid diffusion of ions/electrons, but the energy density is insufficient. Simply increasing the thickness of the cathode will increase the volumetric capacity slightly, but the prolonged and tortuous ion and electron transport pathway will significantly reduce the specific capacity and rate performance of the electrode, thus decreasing the material utilization. Nonetheless, by shaping the high-aspect ratio structures, high active material loading, high areal capacity and efficient mass transport could be secured without compromising the performance of the cell (Fig. 3a).

It has been reported that forming the high-aspect ratio open-lattice architectures by tapping into the height zone is highly efficient to realize high-area capacity electrodes. However, it is laborious and time-consuming to establish such complicated 3D structures using conventional methods. Instead, 3D printing provides a facile approach to building highly complex architectures with internal open channels which facilitate electrolytic infiltration and ion transport within thick electrodes.[58,62,71,72] Meanwhile, 3D printing offers a convenient way to precisely control the thickness of the electrodes, which helps to regulate active material loading and probe the effects.

For instance, Zhang *et al.* designed a porous 3D cathode framework via DIW with a classical SiO_2 template method.[73] The thickness of a single printed layer was 150 μm with a sulfur loading of 2–3 mg cm^{-2}. A high-loading S cathode of 10.2 mg cm^{-2} with a thickness of 600 μm was successfully fabricated by four printed layers. With such a layer-by-layer printing process, a 3D grid skeleton composed of vertical and horizontal structures was constructed. The pores in microscopic scale between the grids allowed good contact between the electrolyte and the active materials. When the as-fabricated S

ARTICLE

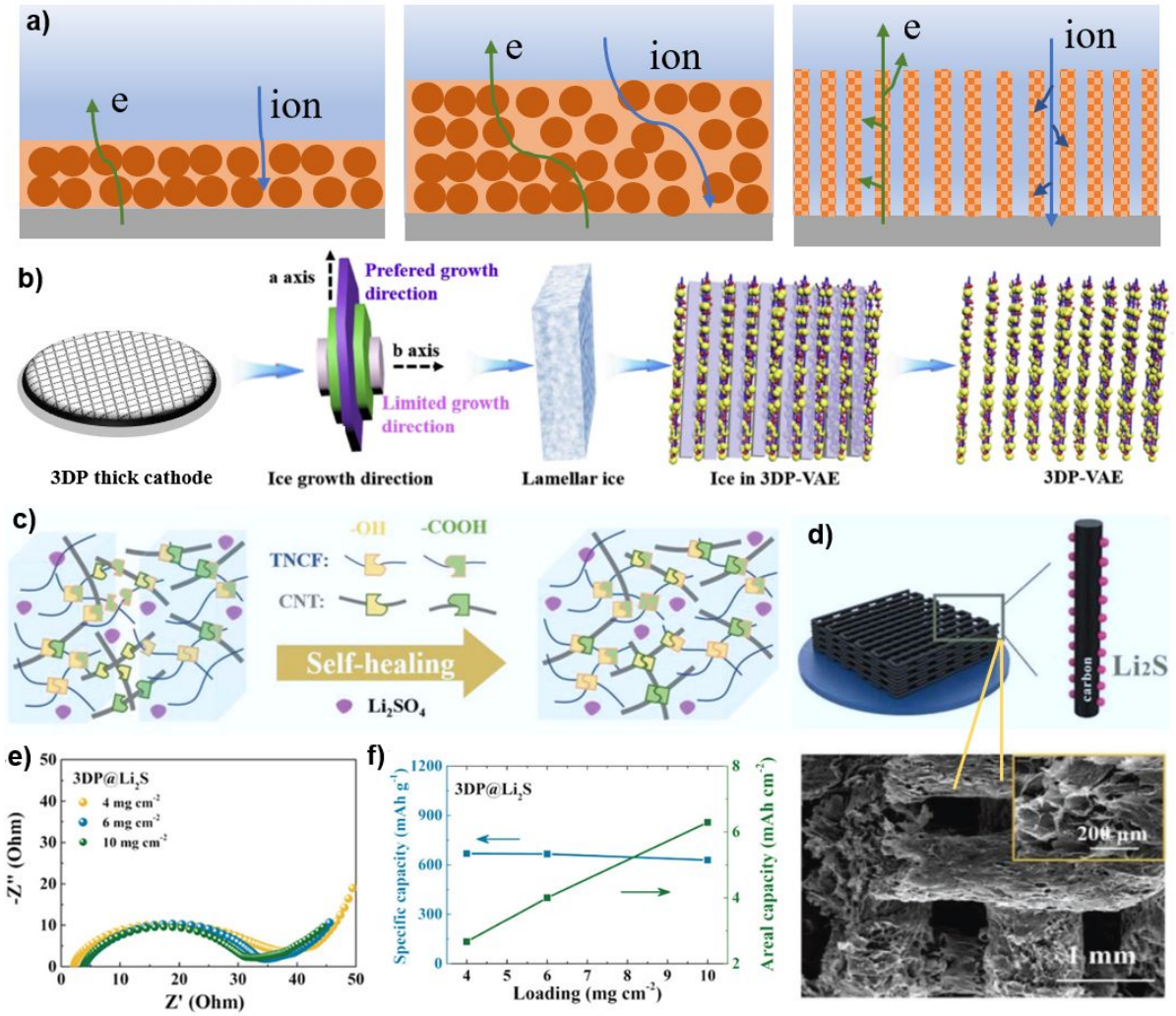

Figure 3. Selected examples of printed cathodes with fast electron and ion transport kinetics. (a) Schematic diagram of electron and ion transport in thin, thick, and 3D-printed cathodes (from left to right). (b) Mechanism for the growth of lamellar ice inside the 3D-printed vertically aligned electrode. The lamellar walls of ice formed in a 3D-printed cathode; the ice grew faster along the a-axis than the b-axis. Finally, vertically aligned "thin electrodes" were fabricated by removing the ice templates. Reproduced with permission.[75] Copyright (2020), Elsevier Ltd. (c) Schematic diagram of the self-healing mechanism of the ink based on dynamic multiple hydrogen bonds, (d) schematic illustration of the 3D-printed Li_2S cathode (upper) and SEM image of the open-lattice structure of the printed cathode (lower), (e) electrochemical impedance spectroscopy (EIS) spectra of 3DP-Li_2S with different active material loadings, and (f) the loading dependence of specific gravimetric and areal capacity of 3DP@Li_2S electrodes at 0.5 C. Reproduced with permission.[76] Copyright (2021), Wiley-VCH GmbH.

cathode was assembled into an Li-S battery, a high reversible discharge specific capacity of 505.4 mA h g^{-1} at 0.2 C with relatively high capacity retention of 78.8% was achieved after 500 cycles. Besides the ability to precisely control the thickness and loading, 3D printing enables the design of complex 3D structures to facilitate mass transport in those thick cathodes, largely improving the electrochemical performance of the batteries.

Sun *et al.* fabricated thick 3D-patterned $LiFePO_4$ (LFP) cathodes with interconnected porous frameworks and continuous conducting carbon networks by an optimized 3D printing technique. To increase the mass loading, the poly(vinylidene fluoride-co-hexafluoropropylene) (PVDF-HFP)

was employed for fully wrapping the nanoparticles. A high-mass loading LFP cathode with homogeneous active material distribution was obtained by combining advantages of porous polymer frameworks and robust 3D structures with a large surface area.[74] The ultra-thick 3D electrode of 1500 μm with eight printed layers showed a high areal capacity of 7.5 mA h cm^{-2} and an energy density of 69.41 J cm^{-2} at a power density of 2.99 mW cm^{-2}, which demonstrated comparable values with reported LFP-based cathodes by both 3D printing and conventional methods in the literature.

The study demonstrated that a thick electrode with high active material loading could be ensured by 3D printing technology. But achieving a thickness-independent cathode is still challenging because Li ion transport is usually poor in thick cathodes. Recently, Sun's group achieved a thickness-independent high-loading S cathode for the first time by combining the 3D printing technology with an ice-template method.[75] The ice was used as an environmentally friendly template for synthesizing the vertical "thin electrodes" in a 3D printed bulk structure based on the crystallographic and anisotropic crystal growth kinetics. Therefore, the fast ice growth along a-axis formed aligned ice walls to divide the thick electrode into numerous vertically-aligned 2D "thin cathodes" with a constant thickness of 20 μm. Assuming a bi-directional transport model, the largest Li^+ diffusion distance of the ultrathin electrodes was no more than 10 μm, which significantly improved the ion transport kinetics (Fig. 3b). It has been shown that the as-fabricated two S cathodes with loadings of 2 and 6 mg cm^{-2} represented similar electrochemical kinetics (i.e., charge transfer resistances, Li^+ diffusion coefficient) and similar electrochemical performance (i.e., rate performance, specific capacity, and cycling stability). Both cathodes exhibited a capacity of 640 mA h g^{-1} at 8 mA cm^{-2} and a low-capacity attenuation of 0.1% per cycle over 200 cycles.

It should be noted that the layer-by-layer printing fabrication process raises the issue of loose contact and large interfacial resistance between the printed layers, especially when using inks with poor fluidity, which can cause large polarization, rapid performance decay and reduced material use. If additional active materials need to be infused into the printed framework, the contact between the active material and the skeleton should be also considered. Moreover, by increasing electrode thickness and active material loading, more challenges like migration, cracking, delamination during post-treatment, and incomplete electrolyte infiltration tend to arise. In this case, interface engineering between the active material and the printed scaffold as well as the printed layers is highly essential.[77] For instance, Zhang *et al.* devised a carbonaceous skeleton for an Li_2S cathode by 3D printing.[76] The printable ink was prepared by dispersing Li_2SO_4, cellulose nanofibrils and carbon nanotubes in water to form a homogenous dispersion (Fig. 3c). It was investigated that as-prepared ink had self-healing property; the viscosity of the ink decreased as the shear rate increased. The unique property of the ink enabled instant interface coalescing between the printed adjacent layers, which eliminated the resistance of electrode and improved the conductivity of the printed cathode. The Li_2S nanoparticles were then deposited in situ on the porous carbonaceous skeleton in the argon atmosphere based on the reaction of $Li_2SO_4 + 2C \rightarrow Li_2S + 2CO_2$ (Fig. 3d). Suppressed material aggregation, intimate contact with the carbon scaffold, and thorough active material utilization were obtained by this in-situ surface decoration method. The high-aspect ratio open-lattice architecture along with the contact interface within the cathode enabled thickness-independent electrochemical performance. The Li_2S cathodes with different loadings (4, 6, or 10 mg cm^{-2}) presented similar curves in electrochemical impedance spectroscopy analysis, which indicated the resistance would not increase with additional printed layers (Fig. 3e). Furthermore, with increased thickness and loading, the specific capacity remained almost constant (about 650 mA h g^{-1}) and the areal capacity increased linearly, which benefited from the tactical ink design and open framework by 3D printing (Fig. 3f). Additionally, the 3D printed Li_2S cathode showed rather stable cycling performance with only 15% capacity decay after 100 cycles, in spite of an exceptional mass loading of 10 mg cm^{-2}.

Similarly, Lewis *et al.* added ethylene glycol and glycerol as humectants for preparing printable inks to promote the bonding between individual layers.[78] Multilayer electrodes with a high-aspect ratio interdigitated walls could be printed up to 16 layers with good structural integrity and stable adhesion between printed features. A graded volatility solvent system was used to control the ink solidification and adhesion during patterning, with water evaporation to maintain the printed structure. Benefiting from the use of ethylene glycol and glycerol, the designed high-aspect ratio structure exhibited strong and stable contact between adjacent layers and showed good adhesion with the substrate after the post-treatment process. The fabricated LFP cathode showed a high specific capacity of 160 mA h g^{-1} that was in good agreement with the theoretical value (170 mA h g^{-1}).

Beside forming a continuous conducting network at the bulk electrodes, another strategy is to prepare inks with nanocomposites of carbon and active materials for printing, which is effective and practical to increase the Li ion and electron transfer in thick electrodes as well as to protect the materials from side reactions at the electrolyte/electrode interface.[74,79] Meanwhile, with the coating of carbon, it is easier to obtain uniform and printable inks, promoting the large-scale production of inks for practical applications of printing techniques. For instance, Kumar *et al*. reported microarchitected nanocomposite cathodes composed of PLA, LFP, and CNT. A grid-like pattern with ordered and controllable porosity was enabled by 3D printing, which helped facilitate sufficient electrolyte penetration and maximize the material utilization.[71] By regulating the content of the CNT, the LFP could be uniformly wrapped around the CNTs with close contact, enabling efficient charge transfer. This work showed the possibility to obtain high specific capacities and high areal capacities at the same time by rationally designing the microstructure of the electrodes.

From the above discussion, both tactical material design in microscale and novel electrode structure construction by 3D printing are necessary. Thick electrode design with a high mass

loading of active materials, excellent electrochemical performance as well as scalable manufacturing will greatly increase the energy density of batteries and reduce the cost of fabrication, which will move the development of SSBs one step closer toward practical applications.

5. Printing strategies for SSEs

A number of studies have shown that the use of SSEs can effectively mitigate safety issues in lithium batteries by providing a physical barrier to the dendrites, thus promoting the development and commercialization of high-energy density Li metal-based SSBs. Generally, SSEs can be divided into two main categories: inorganic (ISEs) and polymeric (SPEs). SPEs typically consist of a polymer host as the solid matrix and a dissolved lithium salt as the lithium-ion conductor, which offers outstanding properties including high flexibility, easy processability, good wettability and low interfacial resistance with electrodes. The softness and elasticity of SPEs enable them to withstand the large volume changes/stresses during cycling without losing contact with the electrodes.

ISEs can be classified into two types: oxide solid electrolytes (e.g., NASICON, perovskites, γ-Li_3PO_4, and garnets) and sulfide solid electrolytes (e.g., Li_2S with SiS_2, P_2S_5, or GeS_2). ISEs are fast lithium-ion conductors and thus have major advantages in conductivity, particularly with the sulfide solid electrolytes achieving conductivities (10^{-5} to 10^{-2} S cm^{-1} at room temperature) comparable to organic based liquid electrolytes and probably greater than those below ambient temperatures. The versatility and unique properties of both ISEs and SPEs widen the applications towards high-energy density Li metal-based batteries. However, there are notable challenges to producing high-ionic conductivity SSEs using current methods such as vacuum-based radio frequency (RF), atomic-layer deposition (ALD), chemical-vapor deposition (CVD), and pulsed-layer deposition (PLD).[28,80] These traditional approaches are either cost-prohibitive, time-consuming, or less scalable. The long sintering time at high temperatures during these processes will inevitably cause severe Li and Na loss in ISEs, leading to low ionic conductivities (~10^{-8} to 10^{-4} S cm^{-1}) and poor electrochemical performance. Besides, common SSB assembly approaches like the tableting or solution-casting method require a specific mold to obtain a designed electrolyte film, which usually has very limited form factors and hinders manufacturing efficiency.

Printing technologies can provide a facile manufacturing method for solving the previously described problems and producing SSEs with customized shapes as well as high conductivities.[81, 82] Cao *et al.* employed DIW to print LATP-based ISEs directly on an $LiFePO_4$ cathode.[34] Customized configurations including "L", "T", and "+" shapes were successfully printed, and the as-fabricated ISEs achieved high ionic conductivity up to 4.24×10^{-4} S cm^{-1}. The solid-state LFP/Li battery assembled with the printed LATP-based SSE delivered a high discharge specific capacity of 150 mA h g^{-1} at 0.5 C and good cycling stability at 60 °C. In this study, a long-term high-temperature sintering process (6 h) after printing was needed, which could not fully present the superiority of applying printing technology in the fabrication process. Integrating printing techniques with other effective fabrication methods is a good choice if post-treatment cannot be waived, which can significantly improve manufacturing efficiency and boost the performance of printed SSEs. For instance, Hu *et al.* developed a "printing and radiative heating" (PRH) approach for fabricating ceramic SSE films directly from the precursors (Fig. 4a).[83] The ceramic precursor inks were printed on various substrates, realizing multifunctional device engineering. Thereafter, a rapid sintering process (~3 s) at 1500°C was conducted to obtain a high-performance $Li_{6.5}La_3Zr_{1.5}Ta_{0.5}O_{12}$ (LLZTO) ceramic SSE film. The thickness of the printed film was well controlled by spray printing to better optimize the sintering temperature and time. The simple printing process integrated with rapid high-temperature sintering (e.g., PRH) enabled the SSEs fabrication time to be shortened to ~5 min. Furthermore, compared to conventional furnace-sintering methods, the PRH process was found to fabricate a dense garnet structure with minimum Li loss and side reactions, thus achieving ceramic SSEs with high Li ionic conductivity (~10^{-3} S cm^{-1}) (Fig. 4b). A solid-state battery was formed by coating $LiCoO_2$ and Li on both sides of the LLZTO pallet separately, which exhibited excellent rate and cycling performance over 450 cycles with a specific capacity of 87 mA h g^{-1} at a current density of 30 mA g^{-1}.

Though ISEs can gain remarkable ionic conductivity after high-temperature sintering, their hard and fragile mechanical properties make it difficult to apply in large-scale SSBs. Moreover, their poor flexibility at the interface increases the risk of high resistance and low interface conductivity. On the other hand, for those SPEs that are soft and easy to process, the low ionic conductivity and poor stability at elevated temperatures limit their applications, as well. In order to build "ideal SSEs", fabricating composite polymer electrolytes (CPEs) by combining ISEs and SPEs shows promise for delivering enhanced properties. Improving the conductivity by adding ceramic fillers to polymer electrolytes will be a good test case to show the synergistic effect of the combination, because the appearance of space charges alignment at the ceramic/polymer electrolyte interface enhances conduction. Fortunately, printing technology provides a convenient tool to control the ceramic-polymer ratio, construct the integrated 3D structure,

ARTICLE

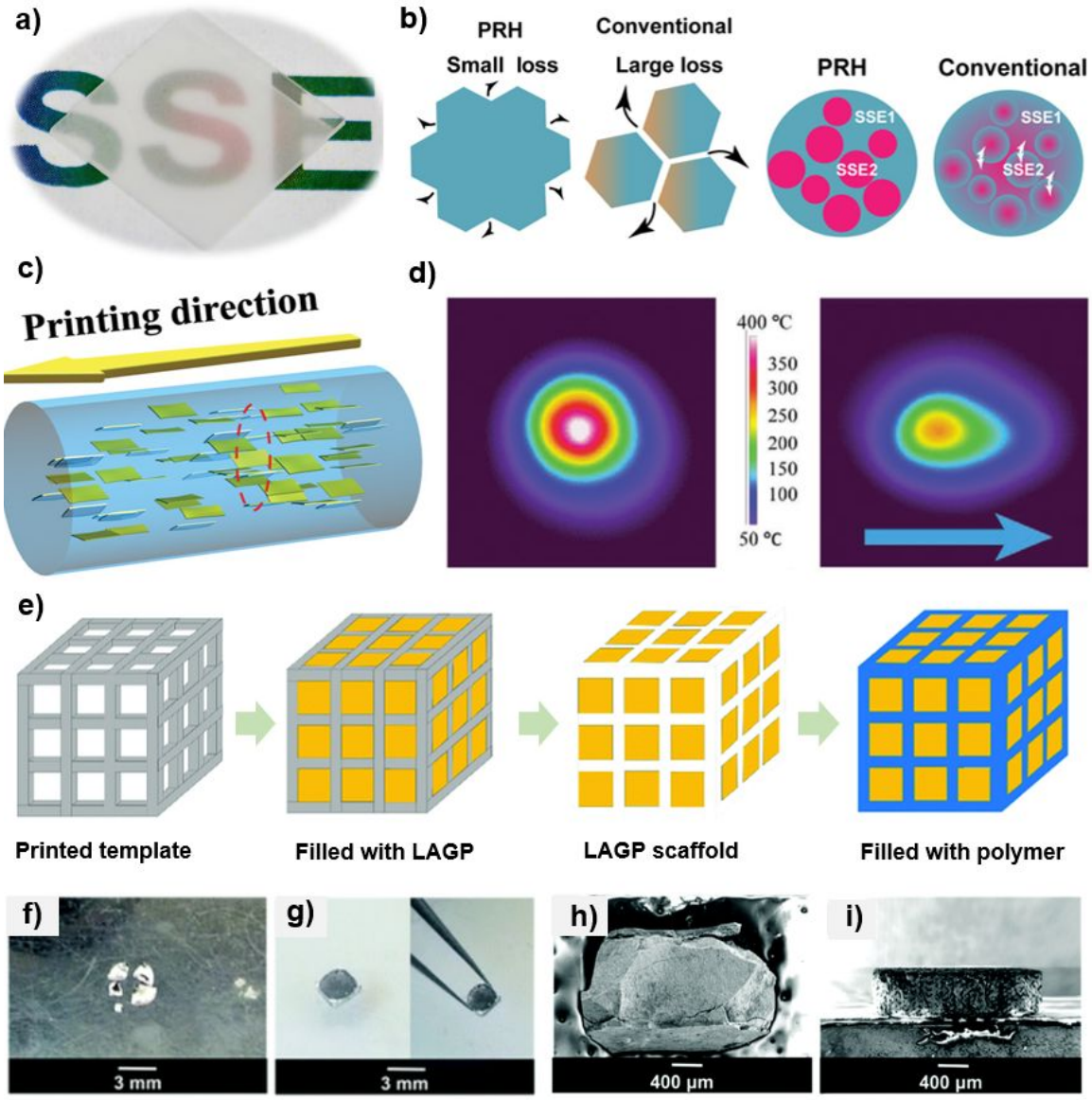

Figure 4. Selected examples of printing SSEs with suitable mechanical strength and high ionic conductivity. (a) Photograph of printed LLZTO garnet film after sintering, and (b) schematic illustration of the side reaction control comparison between PRH and conventional methods.[83] Copyright (2020), American Association for the Advancement of Science. (c) Schematic illustration of the alignment of the hBN platelets in the CPE host along the printing direction, and (d) IR images of the temperature distribution of CPE (left) and CPE with aligned hBN (right) at a laser source power of 100 μW.[85] Copyright (2021), Wiley-VCH GmbH. (e) Schematic illustration of the procedure for synthesizing structured hybrid electrolytes (with the example of the cube microarchitecture), and post-cycling photographs (f-g) and cross-sectional SEM images (h-i) of the LAGP pellet (f, h) and 3D-printed LAGP-CPEs (g, i) after 30 cycles (LAGP pellet) or 40 cycles (3D LAGP-CPEs) at a total areal current density of 0.7 mA cm^{-2}. Reproduced with permission.[86] Copyright (2018), Royal Society of Chemistry.

and possibly align the space charges, thus largely promoting the performance of CPEs for batteries.[84]

Yassar *et al.* found that the inorganic fillers of CPEs could be aligned along the extruding direction by the shear force provided by DIW process.[85] The printable ink with shear-thinning behavior was prepared by adding hexagonal boron nitride (hBN) fillers into a polymeric mixture. With the increased shear rate, the apparent viscosity of the ink decreased, primarily

due to the alignment of both polymer and fillers in the shear direction (Fig. 4c). It has been reported that lithium may be more likely to grow on the hot region than on the surrounding cool region, indicating a promising strategy to reduce the safety issues caused by heat and internal shorting. According to the temperature distribution at the surface of the composites revealed by a micro thermal imaging microscope, CPEs with aligned hBN exhibited a surface temperature 24.2% lower than the CPEs without hBN, and 10.6% lower than that of the CPEs with randomly distributed hBN (Fig. 4d). With the enhanced heat-conduction pathway, the dendrite penetration problem in soft polymer electrolytes can be largely mitigated. An LFP/Li half-cell with printed hBN-based electrolyte exhibited a high specific discharge capacity of 146 mA h g^{-1} and stable cycling performance due to the improved thermal transport for uniform Li deposition. This study has shown that printing technology can change the physical properties of printed materials, thus making it possible to build safer SSBs.

While composites of ceramic and polymer electrolytes offer many benefits, the multiple interfaces introduced between them often impede the ions crossing the interfaces. Consequently, accurately arranging the structure of the CPEs and maintaining continuous pathways for ions are necessary to achieve superior performance. It should be expected that "ideal SSEs" with good safety, suitable mechanical strength, high ionic conductivity, and customized shape can be realized with the assistance of printing technology. Bruce *et al.* designed a novel CPE structure consisting of 3D-ordered bicontinuous interlocking channels by stereolithography (Fig. 4e).[86] First, computationally designed 3D polymer templates with microarchitectures were printed and the empty channels were filled with LAGP powder. After removing the template and sintering the LAGP phase, the structured LAGP scaffold was formed. Finally, the empty channels generated at the removing step were filled with an insulating polymer (epoxy), creating well-designed bicontinuous microchannels. Though insulating polymer was added, the ionic conductivity of the printed LAGP-based CPE reached 2.7×10^{-4} S cm^{-1}, comparable to that of the pure LAGP pellet (2.8×10^{-4} S cm^{-1}). The superior electrochemical performance of the 3D-structured LAGP-based CPE has been attested in the Li symmetric cell, which showed the effective current density was roughly 40% higher than that of the LAGP pellet. The printed hybrid 3D structure also exhibited outstanding mechanical strength and good cycling stability. After 30 cycles, the LAGP pellet cells split into several fragments while the 3D LAGP electrolytes remained in one piece (Fig. 4f-g). More significantly, there was an obvious detachment at the interface for the LAGP pellets, but only minor and partial cracks were noticeable for the printed LAGP electrolytes (Fig. 4h-i). According to the mechanical testing, the 3D-structured LAGP electrolytes showed a fracture strain 28% higher than that of the LACP pellet. This improvement may be due to the strong interfacial interaction between the epoxy polymer and LAGP ceramic, which was promoted by the large surface contact area of the 3D-printed architecture.

6. Printing strategies for addressing interfacial challenges

Despite the significant process in suppressing Li dendrites in anodes, increasing the mass transport in a thick cathode, and constructing SSEs with ideal properties, the sluggish interface kinetics between the SSEs and electrodes still severely limit cell performance when these three components (i.e., anode, cathode and SSE) are assembled. The interfacial issues can be simply understood from physics and chemistry, which correspond to the poor physical contact and side reactions at the electrode interfaces.[87]

On the anode-SSE interface, the physical contact is mainly affected by the mismatch of its surface energies and the volume changes upon the lithiation/delithiation process. As we discussed previously, Li dendrite growth is an indicator of interface problems, primarily due to the poor physical contact and chemical instability. The situation will be more complicated on the cathode-SSE interface, since there are many factors that can significantly affect the contact, including the surface topography of the SSEs and cathodes, the electron conductivity of cathode materials, and the volume variations of cathodes during cycling.[88] The insufficient contact between SSEs and electrodes will give rise to large charge-transfer polarization, increased interfacial resistance, and poor rate performance, resulting in the low-energy density of the full cells. The chemical contact is also an important concern for developing high-performance SSBs, and problems typically include solid passivating film on the anode-SSE interface, Li dendrite growth within the bulk SSEs, and a space-charge zone at the cathode-SSE interface. Therefore, both rational composition design and structure design are indispensable for solving intricated problems at the interface with physical and chemical contact issues. Fortunately, printing technology offers a convenient tool for combining the chemistry and physics by printing favorable structures with reasonably selected materials to tackle physical and chemical problems at the interface simultaneously.[89,90]

ARTICLE

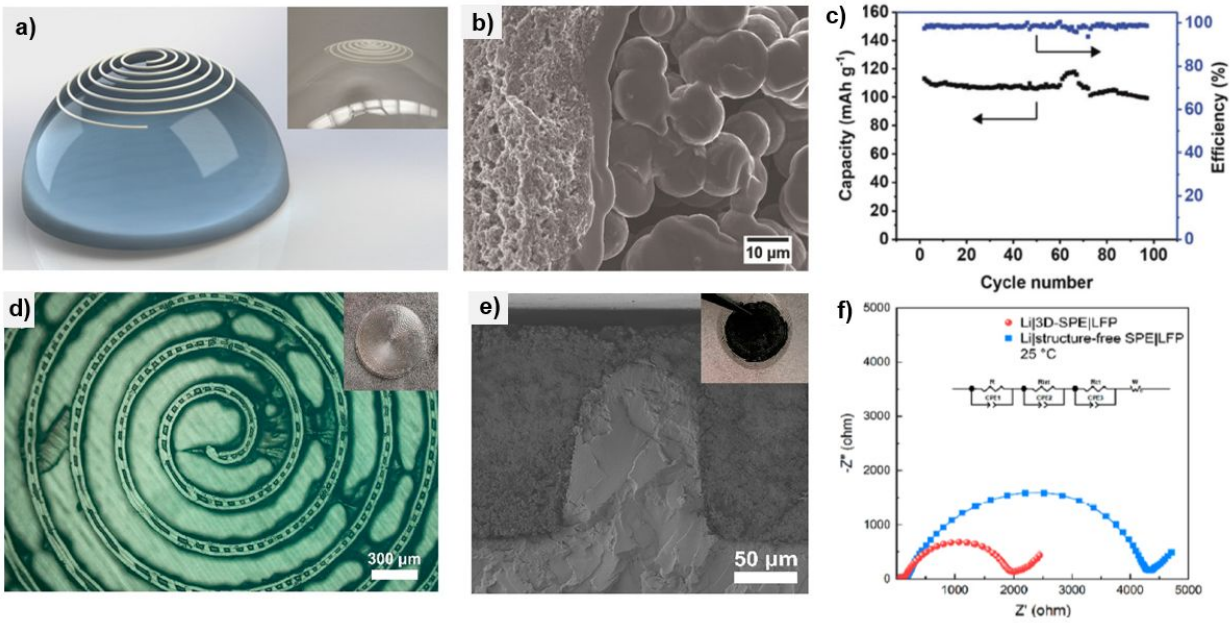

Figure 5. (a) Schematic of a CPE that was printed onto a hemispherical surface, and digital image of the printed electrolyte (inset), (b) SEM image illustrating the dense layer formation between CPE and the MnO_2 electrode, and (c) cycling performance of Li/SSE/MnO_2 at 16 mA g^{-1}.[36] Copyright (2018), WILEY-VCH Verlag GmbH & Co. KGaA. (d) Schematic illustration of the top view of 3D-SPE, (e) cross-sectional SEM image of the integration of the 3D-SPE and electrode, indicating the contact interface between the electrolyte and cathode material (Inserts: digital image), and (f) comparison of the effects of 3D-printed and traditional SSBs on the rate capability by Nyquist plot of a solid-state Li|LFP cell with a 3D-SPE and Li|LFP cell with normal SPE at 25 °C.[42] Copyright (2020), American Chemical Society.

It has been reported several times that the 3D lattice configuration can effectively dissipate high-current densities and achieve low overpotential for Li deposition, and the Li alloys can significantly promote uniform nucleation and growth of Li. To achieve a stable Li-SSE interface, Panat *et al.* combined these two strategies, printing a multifunctional 3D microlattice Ag framework with hierarchically porosity as an Li anode.[91] Besides, an artificial buffer layer at the interface can reduce the interfacial resistance, improve the ion transport rate, and increase the cycling life. Sierros *et al.* printed a 3D porous Cu current collector for accommodating Li metal.[92] The interconnected 3D network provided a large surface area, ensuring sufficient contact between the Li anode and SSEs. The thin layer of CuO between the LATP-based SSE and Cu grid had low electronic conductivity, forming a multifunctional solid electrolyte interphase that could lower the interfacial resistance and overcome the side reactions. The Coulombic efficiencies of the SSBs with a 3D Cu grid maintained above 99% at different current densities during cycling, indicating a stable SEI film and a good (de)lithiation process. Similarly, Yang *et al.* directly printed a 3D LiF scaffold which could form a uniform LiF-rich solid electrolyte interphase, thus enhancing Li ion diffusion rates at the interface.[57] This buffer layer can also be formed during the printing fabrication process. For instance, Yassar and co-workers found that a functional dense layer was created between the porous electrolyte layer and the electrode.[36] By using the DIW, the PVDF-co-HFP-based polymer electrolyte could be directly printed onto the MnO_2 cathode (Fig. 5a). An elevated temperature (120 °C) during the printing process caused the PVDF-co-HFP to melt and thus form a dense layer. Interestingly, this dense layer, which similarly functioned as a binder in the electrode, provided a close contact between the electrolyte and the electrode, according to the SEM image (Fig. 5b). Due to the close contact at the interface, the Coulombic efficiency of the Li/SSE/MnO_2 was maintained at 98.6% for over 100 cycles (Fig. 5c).

ARTICLE

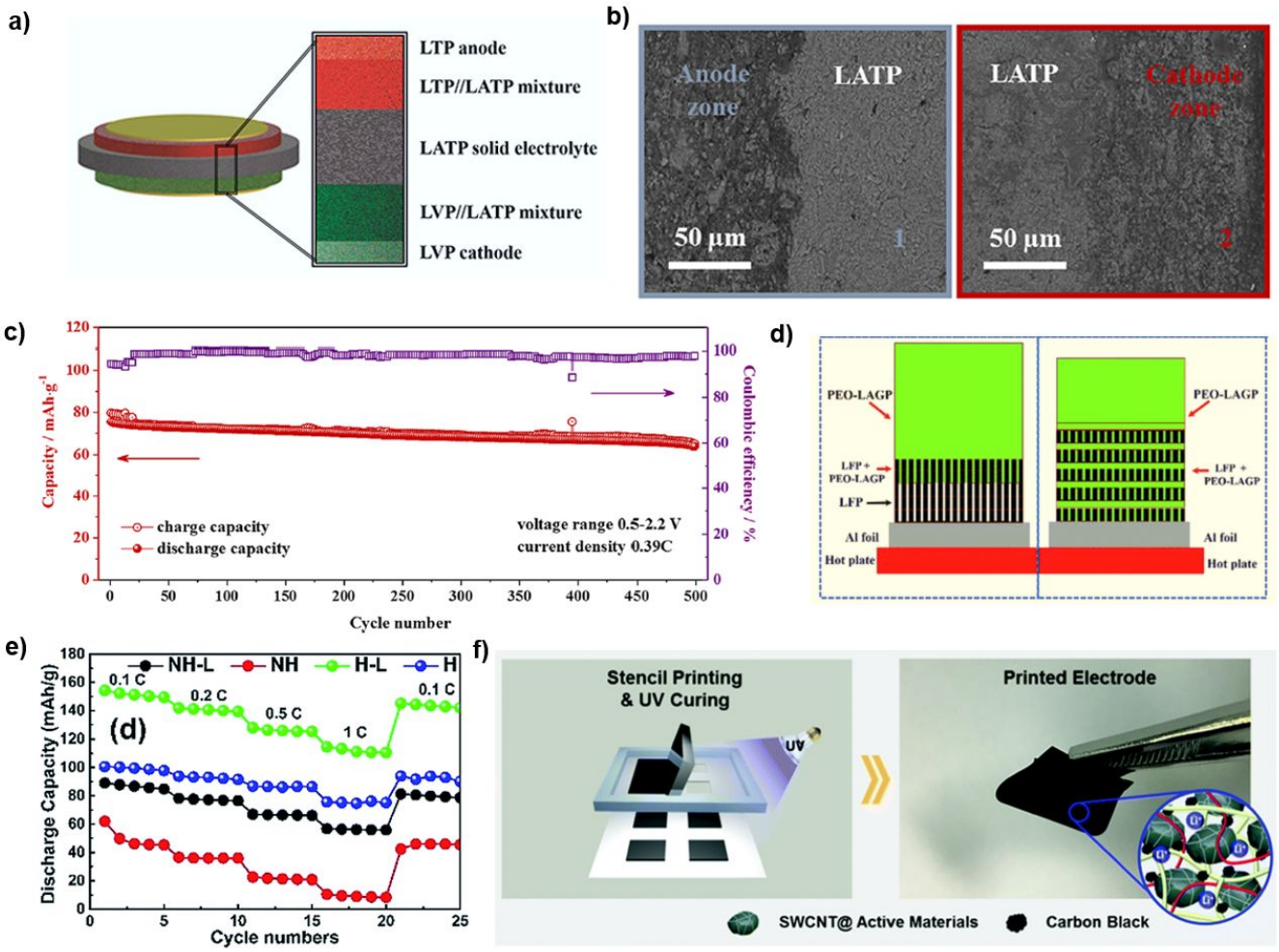

Figure 6. (a) Schematic illustrations of monolithic all-phosphate SSLBs, (b) SEM image demonstrations of interfacial microstructure of the prepared battery, and (c) cycling performance of the SSBs in the voltage range of 0.5–2.2 V at a current density of 0.39 C at 30 °C.[93] Copyright (2018), American Chemical Society. (d) Schematic diagrams of spray-printed honeycomb type and honeycomb-layered type SSEs, showing excellent electrolyte penetration through the electrode provided by the layer-by-layer spray-printing technique, and (e) comparison of the discharge capacities of the printed SSEs honeycomb-layered structure (H-L) with other types at 60 °C.[49] Copyright (2019), Royal Society of Chemistry. (f) Schematic illustration of stencil-printing composite electrodes that consisted of the gel electrolyte, carbon black additive, and active material (left), photographs of the composite electrode (right).[94] Copyright (2018), Royal Society of Chemistry.

In addition to designing structures for electrodes, printing technology provides a facile approach to building 3D pattern SSEs with increased contact area, which is also helpful for reducing the interfacial resistance.[95] Liu *et al.* designed a 3D-SPE with an Archimedean spiral structure via stereolithography printing (Fig. 5d).[42] Compared with structure-free SPE, the unique spiral pattern increased the specific area and improved the interface adhesion between the electrolyte and the electrode (Fig. 5e). The Nyquist plots indicated a total impedance of Li|3D-SPE|LFP cells that was lower than that of Li|structure-free SPE|LFP cells, which contributed to the large and intimate contact area between SPE and LFP (Fig. 5f).

Due to the soft substance and high electronic conductivity of Li metal, a good contact was easily achieved with molten Li, and thus more efforts have been devoted to facilitating the Li ion transport and interface stability. The side reactions at the interface are mainly caused by the incompatible electrodes and electrolyte materials.[81] It has been reported that components with high structural similarity can reduce the interfacial resistance due to the enhanced chemical stability. Eichel *et al.*

developed a monolithic all-phosphate concept by screen-printing $LiTi_2(PO_4)_3$ anode and $Li_3V_2(PO_4)_3$ cathode composites on a densely sintered LATP solid electrolyte (Fig. 6a).[93] The all-phosphate backbone structures effectively avoided chemical side reactions and mitigated chemical interdiffusions at the interfaces of electrodes and SSEs. According to the cross-section SEM images, the SSBs with all-phosphate components showed excellent interfacial matching, either on the anode side or the cathode side. Additionally, the employment of screen printing for composite electrode preparation allowed the composite electrodes to better attach to dense LATP electrolytes by applying a pressure (Fig. 6b). As a result, in the voltage range of 0.5-2.2 V, the SSEs exhibited a highly competitive discharge capacity of 63.5 mA h g^{-1} and outstanding cycling stability (84% capacity retention after 500 cycles) (Fig. 6c). The good performance was attributed to the stable interface, which was enabled by rational material selection and the application of printing technology.

Printing with electrode and SSE composite inks also effectively achieves the intimate contact between active materials and electrolytes throughout repeated cycling. Grant *et al.* investigated a co-spray printing approach to print a composite electrode consisting of $LiFePO_4$ and a PEO-$Li_{1.5}Al_{0.5}Ge_{1.5}(PO_4)_3$ hybrid electrolyte.[49] The co-spray printing offered a facile way to assemble the composite electrode layer by layer, ensuring the solid electrolyte dispersed intimately and continuously into the whole electrode. Additionally, the spray-printed layers had a honeycomb porosity, which enabled the electrolyte to penetrate both within and between layers (Fig. 6d). Due to the superior layered honeycomb structure realized by spray printing, the solid-state half-cell assembled with the composite electrode showed good long-term cycle stability (e.g., 97.2% retention after 100 cycles at 60 °C) and outstanding rate performance, delivering 150 mA h g^{-1} at 0.1 C and 110 mA h g^{-1} at 1 C, largely outperforming that of bulk electrodes without good electrolyte penetration (Fig. 6e). Likewise, Lee *et al.* used stencil printing, which is similar to screen printing, to fabricate composite anodes and cathodes, with pastes prepared with electrode materials and semi-IPN gel electrolytes. The mono full cell assembled with printed $LiCoO_2$, $Li_4Ti_5O_{12}$, and gel electrolyte showed a high specific capacity of 130 mA h g^{-1} and stable cycling behavior with 95% capacity retention after 50 cycles without any internal short-circuit failure.[94] Another flexible/nonflammable sebaconitrile-based gel electrolyte was also incorporated to eliminate the grain-boundary resistance and improve mechanical deformability. UV irradiation was performed to cure the flexible gel network, which then acted as an ion conductor in SSE and binders for electrodes. The integration of the UV curing process with printing technology provided the remarkable advantage of eliminating high-pressure/high-temperature sintering in the traditional electrode preparation process, thus enabling the facile fabrication of solid-state LIBs with various form factors (Fig. 6f).

7. Summary and outlook

The application of printing techniques in batteries has garnered considerable attention, particularly for their scalability, cost-effectiveness, functional versatility, outstanding 2D/3D patterning performance, and superior ability to conveniently combine material chemistry and structure physics. Meanwhile, printing techniques have shown their promising potential for mitigating the critical problems with SSBs by printing challenge-driven structures with rationally selected materials. The printed complex 2D patterns enable an increased surface contact area between electrodes and SSEs, precisely controlled thickness for maximizing the material utilization, and easy assembly and integration with other micro-sized electronic components, while the 3D hierarchical structures provide a large contact area and reliable structural support. These 3D hierarchical structures can decrease the local current density of Li anodes, mitigate Li dendrite growth, provide a stable scaffold for accommodating massive Li, shorten the ion transport pathway, increase active material loading for electrodes, and improve the mechanical strength of CPEs. The printing process itself can also provide additional benefits such as the alignment of particles during the DIW extrusion process and improved attachment between the printed materials and substrates. Overall, printing techniques endow SSBs with greatly enhanced structural diversity, higher areal and volumetric energy densities, and higher power density. However, several challenges regarding the printing technology itself warrant significant attention.

First, the preparation of printable inks with desirable rheology properties as well as optimized performance remains sophisticated. The printing inks should be homogeneous dispersions comprised of active materials, dispersing agents, stabilizers, binders, and solvents. Currently, the active materials that have been applied to produce the electrodes and electrolytes via printing are still quite limited. To achieve higher-energy density SSBs, more novel and mutually compatible materials should be explored for printing. Moreover, to accelerate the commercialization of printed batteries, the materials should be easy to process, air-insensitive, and environmentally friendly. Various additives are typically required to form stable and printable inks with suitable viscosity and specific rheology properties to prevent nozzle clogging; however, the use of additives might inevitably hinder the electrochemical performance of printed materials and lower the concentration of active materials, thus negatively impact the loading of printed structures. Therefore, it is preferred to avoid the use of additives or design and apply the multifunctional additives that can act as either conductive agents for improving the electronic conductivity or as binders for a continuous conductive pathway and preventing migration or cracking issues. Some flammable and volatile organic reagents are frequently used as the solvents and have the largest proportions in inks. These solvents can considerably harm the environment and human health, and thus are unfavorable for large-scale production in industry and commercialized applications for the public. Therefore, it will be highly important to employ green solvents (e.g., water) and

environmentally friendly additives (e.g., cellulose) for printable ink preparation.[96,97]

Second, even though printing provides a convenient method for designing various patterns, the printable inks' formulation, optimal structure design, and optimization of the printing parameters can be very costly and time-consuming. To form printable and stable ink, numerous critical factors such as density, viscosity, concentration, zeta potential, and surface tension must be considered. When new materials or new inks are developed, the printing process optimization should also be performed. However, the traditional One Factor At A Time (OFAT) method can vary only one factor in the ink formulation/printing process at a time and then measure the corresponding outcome, which is laborious and hard to conduct when there are too many factors.[98] Moreover, a good structure design model is also critical for printing, since it will not only ensure printability and reduce the amount of support material, but also help to improve the energy storage performance of the batteries. Nonetheless, the designed patterns are normally iterative and non-optimized, indicating that there is still much room for improvement in printing electrodes and electrolytes. To address these issues, machine learning (ML), as a rising technology, could provide an efficient and cost-saving method to simplify the printing fabrication process.[92] The sequential learning was commonly employed in the optimization of the ink formulation and printing process parameters. The specific boundary constraints for the ink constituents (e.g., active material loadings, binder solution, and humectant) could be determined by analyzing the data in the literature as well as in preliminary experiments. Additionally, some ML models could be used to investigate the effects of different factors on the extrusion flow and thus reveal the major factors in the printing process.[99] Moreover, the ML technique enables feature recommendations to existing CAD models of 3D printing, thus expediting the structure model selection process. [100] Therefore, increasing attention is expected on ML-assisted battery printing in the near future. At the same time, characterization methods to directly present the unique properties of printed structures are very limited. Besides the computational simulation analysis methods, more in-depth experimental verification approaches are needed to determine the reasons and mechanisms for the improved performance.[61,101]

Third, the printing technology should be improved for more convenient battery fabrication. In some cases, the water-free and oxygen-free atmosphere is critical for fabricating a successful Li metal-based battery due to the use of active Li metal and/or moisture-sensitive SSEs, which might require installing the printer in a glovebox. However, due to the limited space in conventional gloveboxes, not all printers are suitable for use in gloveboxes. Thus, it is anticipated that more advanced printing techniques with the ability to print air-sensitive materials by providing an inert atmosphere will allow for a wider material selection and promote the development of fully printed SSBs. Even though printing techniques offer an innovative route for fabricating electrodes and electrolytes with various shapes, it is still difficult to create well-controlled microstructures without post-treatment. There is no doubt that post-annealing is sometimes indispensable for removing additives, creating porous structures, improving the electrical conductivity of electrodes, and enhancing the ionic conductivity of SSEs. However, the long-duration, high-temperature sintering process may destroy the fine-printed structures and cause side reactions. Several examples including printing and radiative heating, elevated-temperature printing, and UV-assisted printing have been discussed in this review, indicating the benefits of the rational combination of printing with other advanced techniques. Even so, extensive research is still needed to improve the printing techniques for the one-step time-efficient fabrication of high-performance SSBs without a complicated post-treatment process.

Fourth, more attention is needed on controlling the solidification of printed structures, since solidification of printed "wet film" has large influence on final structures as well as properties of fabricated devices. Typical solidification methods include annealing, freeze-drying, thermo-/UV curing, and hot plate heating.[77,94] For example, UV curing is effective for solidification of printed polymers, forming robust polymer networks and removing unreacted monomers.[94] However, during the drying process, unexpected collapse, shrinkage, and distortion of printed structures may occur, thereby affecting the printing accuracy, reproducibility as well as the device performance. For instance, a printed cellulose nanofibrils hydrogel with a low concentration shrank up to 50 times in thickness.[102] Without precisely controlling the size and the shape of final devices, the advantages of printing technology will be diminished. Therefore, systematical investigation on the solidification process is highly needed.

Finally, achieving fully printed batteries is still challenging. More research on printing the current collector and packaging materials for batteries is highly desirable. Printing versatile structures with metal powder or carbon material inks with high electronic conductivity is promising for fabricating the current collectors with a large contact surface with electrochemical active materials. Even though electrodes and SSEs can be printed with various patterns, the packaging used for the battery assembly will decide the final shape, which means the advantages of printed customized shapes will be diminished. Therefore, developing printed packaging that matches with the battery chemistry and commercial requirements is highly important, since conventional battery casings are normally rigid, inflexible, or bulky pouches with a large sealing edge. Additionally, the monolithic integration of printed batteries with electronic devices is also meaningful, with the benefits of reduced volume/weight and enhanced design diversity of the integrated devices. However, research on printable batteries is still in its infancy stage, and many challenges regarding the printed battery itself and the reasonable integration with other electronic devices must be addressed.

Although printing technology may not be a panacea for every problem in the realization of solid-state Li batteries, it has shown the capability and advantages in combining the chemistry strategies and structural solutions, enabling new SSBs to provide better performance than conventionally fabricated SSBs. Besides improved energy density and power density, the

printed batteries show the possibility for large-scale production with designed shapes, which will perfectly meet the diversified requirements for society's energy demands. By overcoming problems in the printing fabrication process and obtaining an in-depth understanding of the relationship between printing technology and battery performance, there is great promise that printing techniques will occupy a unique and important position in the production market for SSBs.

Conflicts of interest

There are no conflicts to declare.

Acknowledgements

This work was financially supported by the U.S. National Science Foundation (NSF) Future Manufacturing Program (NSF CMMI-2037026).

References

1 W. Zuo, R. Li, C. Zhou, Y. Li, J. Xia and J. Liu, *Adv. Sci.*, 2017, **4**, 1600539.
2 W. Li, B. Song and A. Manthiram, *Chem. Soc. Rev.*, 2017, **46**, 3006-3059.
3 P. G. Bruce, S. A. Freunberger, L. J. Hardwick and J. M. Tarascon, *Nat. Mater.*, 2011, **11**, 19-29.
4 M. Li, J. Lu, Z. Chen and K. Amine, *Adv. Mater.*, 2018, **30**, 1800561.
5 M. Armand and J.-M. Tarascon, *Nature*, 2008, **451**, 652-657.
6 B. Dunn, H. Kamath and J.-M. Tarascon, *Science*, 2011, **334**, 928-935.
7 N. S. Choi, Z. Chen, S. A. Freunberger, X. Ji, Y. K. Sun, K. Amine, G. Yushin, L. F. Nazar, J. Cho and P. G. Bruce, *Angew. Chem. Int. Ed.*, 2012, **51**, 9994-10024.
8 V. Etacheri, R. Marom, R. Elazari, G. Salitra and D. Aurbach, *Energy Environ. Sci.*, 2011, **4**, 3243.
9 J.-M. Tarascon and M. Armand, *Nature*, 2001, **414**, 359-367.
10 D. Lin, Y. Liu and Y. Cui, *Nat. Nanotechnol.*, 2017, **12**, 194-206.
11 L. Wang, Y. Ye, N. Chen, Y. Huang, L. Li, F. Wu and R. Chen, *Adv. Funct. Mater.*, 2018, **28**, 1800919.
12 D. Lei, K. Shi, H. Ye, Z. Wan, Y. Wang, L. Shen, B. Li, Q.-H. Yang, F. Kang and Y.-B. He, *Adv. Funct. Mater.*, 2018, **28**, 1707570.
13 Y. Liu, P. He and H. Zhou, *Adv. Energy Mater.*, 2018, **8**, 1701602.
14 Y. Sun, N. Liu and Y. Cui, *Nat. Energy*, 2016, **1**, 16071.
15 J. Janek and W. G. Zeier, *Nature Energy*, 2016, **1**, 16141.
16 L. Yue, J. Ma, J. Zhang, J. Zhao, S. Dong, Z. Liu, G. Cui and L. Chen, *Energy Storage Mater.*, 2016, **5**, 139-164.
17 J. C. Bachman, S. Muy, A. Grimaud, H. H. Chang, N. Pour, S. F. Lux, O. Paschos, F. Maglia, S. Lupart, P. Lamp, L. Giordano and Y. Shao-Horn, *Chem. Rev.*, 2016, **116**, 140-162.
18 A. Manuel Stephan and K. S. Nahm, *Polymer*, 2006, **47**, 5952-5964.
19 L. Xu, S. Tang, Y. Cheng, K. Wang, J. Liang, C. Liu, Y.-C. Cao, F. Wei and L. Mai, *Joule*, 2018, **2**, 1991-2015.
20 S. Xia, X. Wu, Z. Zhang, Y. Cui and W. Liu, *Chem*, 2019, **5**, 753-785.
21 Z. Gao, H. Sun, L. Fu, F. Ye, Y. Zhang, W. Luo and Y. Huang, *Adv. Mater.*, 2018, **30**, 1705702.
22 S. Xin, Y. You, S. Wang, H.-C. Gao, Y.-X. Yin and Y.-G. Guo, *ACS Energy Lett.*, 2017, **2**, 1385-1394.
23 Y. Pang, Y. Cao, Y. Chu, M. Liu, K. Snyder, D. MacKenzie and C. Cao, *Adv. Funct. Mater.*, 2019, **30**, 1906244.
24 X. Tian, J. Jin, S. Yuan, C. K. Chua, S. B. Tor and K. Zhou, *Adv. Energy Mater.*, 2017, **7**, 1700127.
25 V. Egorov, U. Gulzar, Y. Zhang, S. Breen and C. O'Dwyer, *Adv. Mater.*, 2020, **32**, 2000556.
26 K.-H. Choi, D. B. Ahn and S.-Y. Lee, *ACS Energy Letters*, 2017, **3**, 220-236.
27 Z. Lyu, G. J. H. Lim, J. J. Koh, Y. Li, Y. Ma, J. Ding, J. Wang, Z. Hu, J. Wang, W. Chen and Y. Chen, *Joule*, 2021, **5**, 89-114.
28 L. J. Deiner, C. A. G. Bezerra, T. G. Howell and A. S. Powell, *Adv. Eng. Mater.*, 2019, **21**, 1900737.
29 P. E. Delannoy, B. Riou, B. Lestriez, D. Guyomard, T. Brousse and J. Le Bideau, *J. Power Sources*, 2015, **274**, 1085-1090.
30 L. J. Deiner and T. L. Reitz, *Adv. Eng. Mater.*, 2017, **19**, 1600878.
31 C. A. Milroy, S. Jang, T. Fujimori, A. Dodabalapur and A. Manthiram, *Small*, 2017, **13**, 1603786.
32 W. J. Hyun, L. E. Chaney, J. R. Downing, A. C. M. de Moraes and M. C. Hersam, *Faraday Discuss.*, 2021, **227**, 92-104.
33 L. J. Deiner, T. Jenkins, T. Howell and M. Rottmayer, *Adv. Eng. Mater.*, 2019, **21**, 1900952.
34 Z. Liu, X. Tian, M. Liu, S. Duan, Y. Ren, H. Ma, K. Tang, J. Shi, S. Hou, H. Jin and G. Cao, *Small*, 2021, **17**, 2002866.
35 M. Wei, F. Zhang, W. Wang, P. Alexandridis, C. Zhou and G. Wu, *J. Power Sources*, 2017, **354**, 134-147.
36 M. Cheng, Y. Jiang, W. Yao, Y. Yuan, R. Deivanayagam, T. Foroozan, Z. Huang, B. Song, R. Rojaee, T. Shokuhfar, Y. Pan, J. Lu and R. Shahbazian-Yassar, *Adv. Mater.*, 2018, **30**, 1800615.
37 A. Maurel, S. Grugeon, B. Fleutot, M. Courty, K. Prashantha, H. Tortajada, M. Armand, S. Panier and L. Dupont, *Sci. Rep.*, 2019, **9**, 18031.
38 A. Maurel, M. Courty, B. Fleutot, H. Tortajada, K. Prashantha, M. Armand, S. Grugeon, S. Panier and L. Dupont, *Chem. Mater.*, 2018, **30**, 7484-7493.
39 A. Maurel, M. Armand, S. Grugeon, B. Fleutot, C. Davoisne, H. Tortajada, M. Courty, S. Panier and L. Dupont, *J. Electrochem. Soc.*, 2020, **167**, 070536.
40 H. Ragones, A. Vinegrad, G. Ardel, M. Goor, Y. Kamir, M. M. Dorfman, A. Gladkikh and D. Golodnitsky, *J. Electrochem. Soc.*, 2019, **167**, 070503.
41 Q. Chen, R. Xu, Z. He, K. Zhao and L. Pan, *J. Electrochem. Soc.*, 2017, **164**, 1852-1857.
42 Y. He, S. Chen, L. Nie, Z. Sun, X. Wu and W. Liu, *Nano Lett.*, 2020, **20**, 7136-7143.
43 K. Zehbe, A. Lange and A. Taubert, *Energy Fuels*, 2019, **33**, 12885-12893.
44 J. Gao, C. Chen, Q. Dong, J. Dai, Y. Yao, T. Li, A. Rundlett, R. Wang, C. Wang and L. Hu, *Adv. Mater.*, 2021, **33**, 2005305.
45 S. H. Lee, C. Huang and P. S. Grant, *Nano Energy*, 2019, **61**, 96-103.
46 S. H. Lee, A. Mahadevegowda, C. Huang, J. D. Evans and P. S. Grant, *J. Mater. Chem. A*, 2018, **6**, 13133-13141.
47 S. H. Lee, K. Li, C. Huang, J. D. Evans and P. S. Grant, *ACS Appl. Mater. Interfaces*, 2019, **11**, 603-612.
48 P. Leung, J. Bu, P. Quijano Velasco, M. R. Roberts, N. Grobert and P. S. Grant, *Adv. Energy Mater.*, 2019, **9**, 1901418.
49 J. Bu, P. Leung, C. Huang, S. H. Lee and P. S. Grant, *J. Mater. Chem. A*, 2019, **7**, 19094-19103.

50 M.-S. Park, S.-H. Hyun and S.-C. Nam, *Electrochim. Acta*, 2007, **52**, 7895-7902.
51 J. Y. Kim, D. O. Shin, S.-H. Kim, J. H. Lee, K. M. Kim, J. Oh, J. Kim, M. J. Lee, Y.-S. Yang, S.-Y. Lee, J. Y. Kim and Y.-G. Lee, *J. Power Sources*, 2018, **401**, 126-134.
52 H.-D. Um, K.-H. Choi, I. Hwang, S.-H. Kim, K. Seo and S.-Y. Lee, *Energy Environ. Sci.*, 2017, **10**, 931-940.
53 J. Sastre, M. H. Futscher, L. Pompizi, A. Aribia, A. Priebe, J. Overbeck, M. Stiefel, A. N. Tiwari and Y. E. Romanyuk, *Commun. Mater.*, 2021, **2**, 76.
54 H. Liu, X.-B. Cheng, J.-Q. Huang, H. Yuan, Y. Lu, C. Yan, G.-L. Zhu, R. Xu, C.-Z. Zhao, L.-P. Hou, C. He, S. Kaskel and Q. Zhang, *ACS Energy Lett.*, 2020, **5**, 833-843.
55 D. Cao, X. Sun, Q. Li, A. Natan, P. Xiang and H. Zhu, *Matter*, 2020, **3**, 57-94.
56 Z. Lyu, G. J. H. Lim, R. Guo, Z. Pan, X. Zhang, H. Zhang, Z. He, S. Adams, W. Chen, J. Ding and J. Wang, *Energy Storage Mater.*, 2020, **24**, 336-342.
57 K. Shen, Z. Cao, Y. Shi, Y. Zhang, B. Li and S. Yang, *Energy Storage Mater.*, 2021, **35**, 108-113.
58 X. Gao, X. Yang, S. Wang, Q. Sun, C. Zhao, X. Li, J. Liang, M. Zheng, Y. Zhao, J. Wang, M. Li, R. Li, T.-K. Sham and X. Sun, *J. Mater. Chem. A*, 2020, **8**, 278-286.
59 W. Zhang, J. Li, H. Chen, H. Jin, P. Li, Y. Zhang, C. Xu, S. Zhao, Y. Du and J. Zhang, *Nano*, 2020, **15**, 2050033.
60 X. Gao, X. Yang, K. Adair, X. Li, J. Liang, Q. Sun, Y. Zhao, R. Li, T. K. Sham and X. Sun, *Adv. Energy Mater.*, 2020, **10**, 1903753.
61 D. Cao, Y. Xing, K. Tantratian, X. Wang, Y. Ma, A. Mukhopadhyay, Z. Cheng, Q. Zhang, Y. Jiao, L. Chen and H. Zhu, *Adv. Mater.*, 2019, **31**, 1807313.
62 C. Chen, S. Li, P. H. L. Notten, Y. Zhang, Q. Hao, X. Zhang and W. Lei, *ACS Appl. Mater. Interfaces*, 2021, **13**, 24785-24794.
63 G. J. H. Lim, Z. Lyu, X. Zhang, J. J. Koh, Y. Zhang, C. He, S. Adams, J. Wang and J. Ding, *J. Mater. Chem. A*, 2020, **8**, 9058-9067.
64 K. Shen, B. Li and S. Yang, *Energy Storage Mater.*, 2020, **24**, 670-675.
65 Y. Liu, Y. Qiao, Y. Zhang, Z. Yang, T. Gao, D. Kirsch, B. Liu, J. Song, B. Yang and L. Hu, *Energy Storage Mater.*, 2018, **12**, 197-203.
66 S. K. Cho, H. I. Kim, J. W. An, K. Jung, H. Bae, J. H. Kim, T. Yim and S. Y. Lee, *Adv. Funct. Mater.*, 2020, **30**.
67 D. Lee, S. Sun, J. Kwon, H. Park, M. Jang, E. Park, B. Son, Y. Jung, T. Song and U. Paik, *Adv. Mater.*, 2020, **32**, 1905573.
68 S. M. Hosseini, A. Varzi, S. Ito, Y. Aihara and S. Passerini, *Energy Storage Mater.*, 2020, **27**, 61-68.
69 T. Shi, Q. Tu, Y. Tian, Y. Xiao, L. J. Miara, O. Kononova and G. Ceder, *Adv. Energy Mater.*, 2019, **10**, 1902881.
70 Y. Kato, S. Shiotani, K. Morita, K. Suzuki, M. Hirayama and R. Kanno, *J. Phys. Chem. Lett.*, 2018, **9**, 607-613.
71 V. Gupta, F. Alam, P. Verma, A. M. Kannan and S. Kumar, *J. Power Sources*, 2021, **494**, 229625.
72 C. Shen, T. Wang, X. Xu and X. Tian, *Electrochim. Acta*, 2020, **349**, 136331.
73 C. Chen, J. Jiang, W. He, W. Lei, Q. Hao and X. Zhang, *Adv. Funct. Mater.*, 2020, **30**, 1909469.
74 J. Wang, Q. Sun, X. Gao, C. Wang, W. Li, F. B. Holness, M. Zheng, R. Li, A. D. Price, X. Sun, T. K. Sham and X. Sun, *ACS Appl. Mater. Interfaces*, 2018, **10**, 39794-39801.
75 X. Gao, X. Yang, Q. Sun, J. Luo, J. Liang, W. Li, J. Wang, S. Wang, M. Li, R. Li, T.-K. Sham and X. Sun, *Energy Storage Mater.*, 2020, **24**, 682-688.
76 L. Xue, L. Zeng, W. Kang, H. Chen, Y. Hu, Y. Li, W. Chen, T. Lei, Y. Yan, C. Yang, A. Hu, X. Wang, J. Xiong and C. Zhang, *Adv. Energy Mater.*, 2021, **11**, 2100420.
77 K. Sun, T. S. Wei, B. Y. Ahn, J. Y. Seo, S. J. Dillon and J. A. Lewis, *Adv. Mater.*, 2013, **25**, 4539-4543.
78 T. S. Wei, B. Y. Ahn, J. Grotto and J. A. Lewis, *Adv. Mater.*, 2018, **30**, 1703027.
79 H. Joachin, T. Kaun, K. Zaghib and J. Prakash, *J. Electrochem. Soc.*, 2009, **156**.
80 A. Chen, C. Qu, Y. Shi and F. Shi, *Front. Energy Res.*, 2020, **8**, 571440.
81 S. H. Kim, J. H. Kim, S. J. Cho and S. Y. Lee, *Adv. Energy Mater.*, 2019, **9**, 1901841.
82 S. Muench, R. Burges, A. Lex-Balducci, J. C. Brendel, M. Jäger, C. Friebe, A. Wild and U. S. Schubert, *Energy Storage Mater.*, 2020, **25**, 750-755.
83 W. Ping, C. Wang, R. Wang, Q. Dong, Z. Lin, A. Brozena, J. Dai, J. Luo and L. Hu, *Sci. Adv.*, 2020, **6**, eabc8641.
84 S. H. Kim, K. H. Choi, S. J. Cho, S. Choi, S. Park and S. Y. Lee, *Nano Lett.*, 2015, **15**, 5168-5177.
85 M. Cheng, A. Ramasubramanian, M. G. Rasul, Y. Jiang, Y. Yuan, T. Foroozan, R. Deivanayagam, M. Tamadoni Saray, R. Rojaee, B. Song, V. R. Yurkiv, Y. Pan, F. Mashayek and R. Shahbazian‐Yassar, *Adv. Funct. Mater.*, 2020, **31**, 2006683.
86 S. Zekoll, C. Marriner-Edwards, A. K. O. Hekselman, J. Kasemchainan, C. Kuss, D. E. J. Armstrong, D. Cai, R. J. Wallace, F. H. Richter, J. H. J. Thijssen and P. G. Bruce, *Energy Environ. Sci.*, 2018, **11**, 185-201.
87 S. Lou, F. Zhang, C. Fu, M. Chen, Y. Ma, G. Yin and J. Wang, *Adv. Mater.*, 2021, **33**, 2000721.
88 S. Lou, Q. Liu, F. Zhang, Q. Liu, Z. Yu, T. Mu, Y. Zhao, J. Borovilas, Y. Chen, M. Ge, X. Xiao, W. K. Lee, G. Yin, Y. Yang, X. Sun and J. Wang, *Nat. Commun.*, 2020, **11**, 5700.
89 S. Ohta, S. Komagata, J. Seki, T. Saeki, S. Morishita and T. Asaoka, *J. Power Sources*, 2013, **238**, 53-56.
90 S. Moon, J.-K. Yoo, Y. H. Jung, J.-H. Kim, Y. S. Jung and D. K. Kim, *J. Electrochem. Soc.*, 2017, **164**, 6417-6421.
91 M. S. Saleh, J. Li, J. Park and R. Panat, *Addit. Manuf.*, 2018, **23**, 70-78.
92 D. Cipollone, H. Yang, F. Yang, J. Bright, B. Liu, N. Winch, N. Wu and K. A. Sierros, *J. Mater. Process. Technol.*, 2021, **295**, 117159.
93 S. Yu, A. Mertens, H. Tempel, R. Schierholz, H. Kungl and R. A. Eichel, *ACS Appl. Mater. Interfaces*, 2018, **10**, 22264-22277.
94 S.-H. Kim, K.-H. Choi, S.-J. Cho, J. Yoo, S.-S. Lee and S.-Y. Lee, *Energy Environ. Sci.*, 2018, **11**, 321-330.
95 D. W. McOwen, S. Xu, Y. Gong, Y. Wen, G. L. Godbey, J. E. Gritton, T. R. Hamann, J. Dai, G. T. Hitz, L. Hu and E. D. Wachsman, *Adv. Mater.*, 2018, **30**, 1707132.
96 S. D. Lacey, D. J. Kirsch, Y. Li, J. T. Morgenstern, B. C. Zarket, Y. Yao, J. Dai, L. Q. Garcia, B. Liu, T. Gao, S. Xu, S. R. Raghavan, J. W. Connell, Y. Lin and L. Hu, *Adv. Mater.*, 2018, **30**, 1705651.
97 R. Gonçalves, J. Oliveira, M. P. Silva, P. Costa, L. Hilliou, M. M. Silva, C. M. Costa and S. Lanceros-Méndez, *ACS Appl. Energy Mater.*, 2018, **1**, 3331-3341.
98 G. D. Goh, S. L. Sing and W. Y. Yeong, *Artif. Intell. Rev.*, 2020, **54**, 63-94.
99 Z. Liu, M. Li, Y. Weng, Y. Qian, T. N. Wong and M. J. Tan, *Compos. B.*, 2020, **193**, 108018.
100 X. Yao, S. K. Moon and G. Bi, *Rapid Prototyp. J.*, 2017, **23**, 983-997.

101 D. Miranda, C. M. Costa, A. M. Almeida and S. Lanceros-Méndez, *Energy*, 2018, **149**, 262-278.

102 K. M. O. Håkansson, I. C. Henriksson, C. de la Peña Vázquez, V. Kuzmenko, K. Markstedt, P. Enoksson and P. Gatenholm, *Adv. Mater. Technol.*, 2016, **1**, 1600096.